Journal of Alloys and Compounds 509 (2011) 2879–2884

Contents lists available at ScienceDirect

Journal of Alloys and Compounds

journal homepage: www.elsevier.com/locate/jallcom

Enhanced mechanical properties of Mg–Gd–Y–Zr casting via friction stir processing

B.L. Xiao, Q. Yang, J. Yang, W.G. Wang, G.M. Xie[1], Z.Y. Ma*

Shenyang National Laboratory for Materials Science, Institute of Metal Research, Chinese Academy of Sciences, 72 Wenhua Road, Shenyang 110016, China

ARTICLE INFO

Article history:
Received 13 August 2010
Received in revised form
22 November 2010
Accepted 22 November 2010
Available online 30 November 2010

Keywords:
Friction stir processing
Magnesium alloys
Solution
Microstructures
Precipitate

ABSTRACT

Mg–10Gd–3Y–0.5Zr casting was subjected to friction stir processing (FSP) at a tool rotation rate of 800 rpm and a traverse speed of 50 mm/min. FSP resulted in the fundamental dissolution of the coarse network-like β-Mg_5(Gd,Y) phase and remarkable grain refinement (~6.1 μm), thereby significantly improving the strength and ductility of the casting. Post-FSP aging resulted in the precipitation of fine β″ and β′ particles in a fine-grained magnesium matrix, producing an ultimate tensile strength of 439 MPa and a yield strength of 330 MPa. FSP combined with aging is a simple and effective approach to enhancing the mechanical properties of Mg–Gd–Y–Zr casting.

1. Introduction

Magnesium alloys with rare earth metals have received a tremendous amount of attention due to their low density and good mechanical properties, such as high strength at room and elevated temperatures and creep resistance [1–5]. Among them, the Mg–Gd–Y system is especially attractive because of its superior heat resistance due to the high melting point intermetallic Mg_5(Gd,Y). An exponential drop of the high equilibrium solid solubility of Gd with decreasing temperature produces an ideal precipitation strengthening [6,7], in addition to the solid solution strengthening [8]. In the past few years, the precipitation behavior, micro alloying, and heat treatment have been widely studied, laying a foundation for optimizing the mechanical properties of the Mg–Gd–Y alloys [1,3,9–12].

At present, the Mg–Gd–Y alloys are supplied mainly in the form of casting. Generally, the as-cast Mg–Gd–Y alloys are characterized by a network of coarse eutectics of Mg_5(Gd,Y) and α-Mg, thus they are very brittle. A solution treatment at a high temperature (~500 °C) for an extended period of time with subsequent aging is necessary for modifying the distribution and morphology of the eutectic network. However, the high-temperature solution treatment results in not only increased material cost but also obvious surface oxidation and grain growth. By comparison, plastic working could refine the grain structure and the precipitates of Mg–Gd–Y alloys significantly, therefore improving mechanical properties, especially ductility [13–15]. Hou et al. [13] reported that an extruded Mg–8Gd–2Y–1Nd–0.3Zn–0.6Zr sheet exhibited an elongation up to 14.2% at room temperature, while ultimate tensile strength and yield strength were 376 and 270 MPa. Moreover, Zhang et al. [14] found that extruded the Mg–Gd–Y–Zr alloy exhibited superplasticity. However, considering the brittleness of the as-cast alloys, it is hard to perform the extrusion or rolling directly on the ingots without a pre-homogenization temper. Thus, developing a short-route working technique for microstructural modification of Mg–Gd–Y alloys is important for widening their applications.

Friction stir processing (FSP), developed based on the basic principles of friction stir welding (FSW) [16,17], is a relatively new working technique for microstructural modification [18]. FSP investigations on the magnesium based alloys have demonstrated that effective microstructural homogenization and refinement could be achieved as a result of severe plastic deformation and dynamic recrystallization (DRX) [19,20]. Investigations of AZ91D and AZ80 castings indicated that FSP resulted in significant breakup and dissolution of the coarse, network-like eutectic β-$Mg_{17}Al_{12}$ phase distributed at the grain boundaries and remarkable grain refinement, producing a fine-grained supersaturated solid solution. A post-FSP aging then resulted in the precipitation of the fine β-$Mg_{17}Al_{12}$ particles, enhancing the mechanical properties of the AZ91 and AZ80 castings significantly [21–23].

* Corresponding author. Tel.: +86 24 83978908; fax: +86 24 83978908.
E-mail address: zyma@imr.ac.cn (Z.Y. Ma).
[1] Now is with Northeastern University, Shenyang 110004, China.

0925-8388/$ – see front matter © 2010 Elsevier B.V. All rights reserved.
doi:10.1016/j.jallcom.2010.11.147

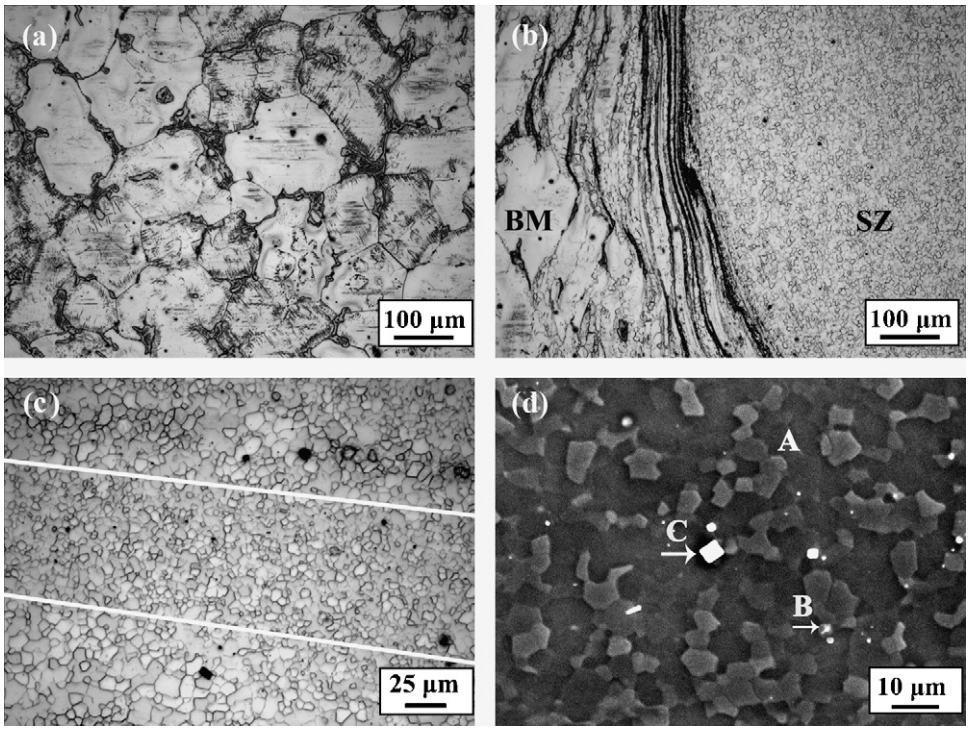

Fig. 1. Microstructure of GW103 samples: (a) as-cast, (b) near SZ of as-FSP, (c) SZ of as-FSP, (d) SZ of as-FSP (SEM image).

Considering the fact that the Mg–Gd–Y alloys, such as Mg–10Gd–3Y–0.5Zr (GW103), contain a great number of thermally stable $Mg_5(Gd,Y)$ particles, it would be very interesting to know whether FSP could achieve the dissolution of the coarse heat-resistant intermetallic particles in the Mg–Gd–Y casting as in the Mg–Al–Zn castings [21–23]. Recently, Freeney et al. [24] reported that FSP enhanced the mechanical properties of a cast Mg–Zn–Nd–Gd–Zr alloy (ASTM EV31A, patented by Magnesium Elektron) due to grain refinement, breakage and dissolution of second-phase particles. However, the evolution of the precipitates containing Gd during FSP was not specified. In addition, the Gd content of the EV31A alloy is much lower (1.7 wt.%) than that of the GW103 alloy. Therefore, it is worthwhile to examine whether FSP can achieve the dissolution of the high content of coarse network-like $Mg_5(Gd,Y)$ phase in the GW103 alloy. In this paper, the effect of FSP on the microstructure and mechanical properties of the GW103 casting was investigated. The aim is to establish a simple and effective approach to enhancing the mechanical properties of the Mg–Gd–Y casting.

2. Experimental

8 mm thick plates cut from a GW103 cast billet (Base material, BM) with a nominal composition of Mg–10Gd–3Y–0.5Zr (wt.%) were used in this study. A tool with a shoulder 20 mm in diameter and a threaded cone pin 8 mm in diameter and 6 mm in length was used. One-pass FSP was performed at a tool rotation rate of 800 rpm and a traverse speed of 50 mm/min (hereafter denoted as 800/50 for short). After FSP, parts of the samples were subjected to artificial aging at 225 °C for 13 h.

The specimens used for microstructural examinations were cross sectioned perpendicular to the FSP direction. Microstructural characterization and analyses were carried out by X-ray diffraction (XRD), optical microscopy (OM), scanning electron microscopy (SEM) complemented by energy-dispersive spectroscopy (EDS), transmission electron microscopy (TEM), and differential scanning calorimetry (DSC). The specimens for OM and SEM were prepared by mechanical polishing and etching using a solution of 4% HNO_3 and 96% ethanol. Thin foils for TEM were ion-milled by a PIPS691 miller at a voltage of 4 kV. The grain size was estimated using the linear intercept method.

The Vickers microhardness tests were performed on the cross-section perpendicular to the FSP direction using a 200 g load for 10 s. Tensile specimens with a gauge length of 25 mm, a width of 4 mm and a thickness of 2.5 mm were machined parallel to the FSP direction with the gauge completely within the stir zone (SZ). Tensile tests were performed using an INSTRON 5848 mini tester at a strain rate of $1 \times 10^{-3}\ s^{-1}$. The tensile fracture surfaces were examined under an SEM.

3. Results and discussion

OM examinations indicated that the microstructure of the as-cast GW103 alloy consisted of approximately equiaxed α-Mg dendrites and the net-shaped divorced eutectics of α-Mg and intermetallic phases around the dendrites (Fig. 1(a)). Furthermore, small platelet-like precipitates near the eutectics were found within the α-Mg grains. XRD patterns revealed that the intermetallic phases were β-$Mg_5(Gd,Y)$ (Fig. 2(a)). The average grain size of the α-Mg in the as-cast sample was about 145 μm. After FSP, the microstructure of the SZ was characterized by fine and equiaxed α-Mg grains (Fig. 1(b)). This indicates that DRX occurred during FSP, leading to significant grain refinement. The average grain size in the SZ was determined to be 6.1 μm. However, OM examinations indicated

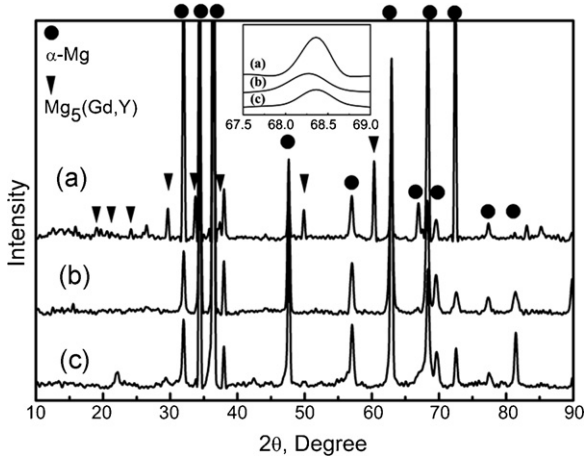

Fig. 2. XRD patterns of GW103 samples: (a) as-cast, (b) as-FSP, (c) FSP + aging.

Table 1
The results of EDS analyses of Fig. 1(d) (wt.%).

Location	Mg	Gd	Y	Zr	O
A	87.87	9.41	2.72	–	–
B	28.19	–	–	28.34	43.47
C	4.37	61.17	34.47	–	–

Table 2
Crystal lattice parameters of pure Mg and GW103 samples under various conditions.

Materials	*a* (Å)	*c* (Å)	*c*/*a*
Pure Mg	3.2090	5.2102	1.6236
As-cast GW103	3.2239	5.2140	1.6173
As-FSP GW103	3.2256	5.2174	1.6175

that the grain size in the SZ was not completely uniform. Alternating coarse grain bands (CGBs) and fine grain bands (FGBs) were observed, as marked by the white lines in Fig. 1(c). Similar observations have been previously reported in FSW copper and FSW aluminum [25,26]. The alternating CGBs and FGBs were macroscopically represented by the onion rings [25], typical structures found on the SZ of FSW/FSP materials [16].

In addition to significant grain refinement, another microstructural characteristic of the FSP GW103 is that no β-Mg_5(Gd,Y) phase was detected under OM even at a high level of magnification (Fig. 1(c)), and the corresponding diffraction peaks disappeared in the XRD patterns (Fig. 2(b)). Fig. 1(b) shows that the net-shaped eutectics were stretched into particle bands at edge of the SZ, indicating the breakup of the eutectics in the SZ. EDS analyses showed that the grain interior of the SZ contained ~9.41 wt.% Gd and 2.72 wt.% Y (Fig. 1(d) and Table 1), which were much higher than the content in the as-cast sample (4.75 wt.% Gd and 1.93 wt.% Y) and close to the chemical compositions of the as-received alloy. These results indicate that the coarse Mg_5(Gd,Y) particles in the as-cast sample were fundamentally dissolved into the magnesium matrix during FSP.

XRD analyses also revealed that the peaks of α-Mg in the SZ (hereafter referred to as the as-FSP sample) shifted toward the lower angle region compared to those in the BM (as shown by the insert in Fig. 2), indicating a change in the lattice parameters. Table 2 shows that compared to those of pure magnesium and the as-cast sample, the crystal lattice parameters *a* and *c* of the as-FSP samples exhibited a remarkable expansion, though the ratio of *c*-axis to *a*-axis of the as-FSP sample was very close to that of the as-cast sample. Fig. 3 shows the relationship between the crystal lattice parameters and the Gd + Y concentration in the magnesium matrix determined by EDS. The crystal lattice parameters of the as-FSP sample tend to increase with increasing the concentration of the dissolved Gd and Y. The atomic radius of Gd (0.25 nm) and Y (0.22 nm) are much larger than that of magnesium (0.17 nm). The dissolution of Gd and Y into the magnesium matrix resulted in an expansion in the crystal lattice parameters of the magnesium solid solution. The data of lattice parameters in Table 2 is in good agreement with an earlier report [27]. Therefore, the expansion in the crystal lattice parameters further proved that FSP resulted in the fundamental dissolution of the Mg_5(Gd,Y) phase.

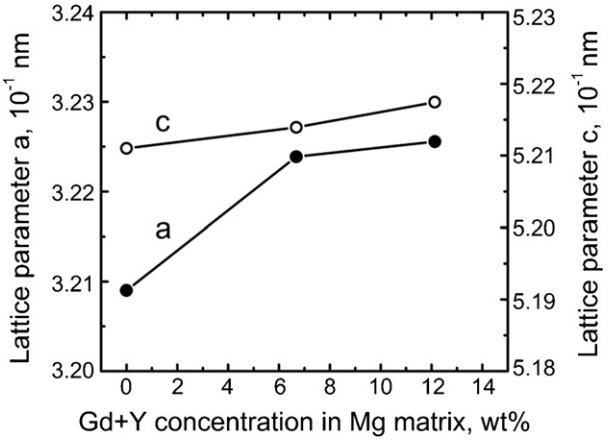

Fig. 3. Relationship between crystal lattice parameters and Gd + Y concentration.

The eutectic point of the Mg–Gd alloy system is 548 °C, so conventional T4 treatment was performed at high temperatures around 500 °C for several hours [3,15]. According to the previous investigations on FSP of Mg alloys, the duration at above 300 °C was only about 20 s [19,28]. Chang et al. [19] reported that a maximum temperature of ~420 °C was recorded in a position 1.5 mm from the SZ during FSP of AZ31 at rotation rates up to 1800 rpm and a constant traverse speed of 90 mm/min. The fundamental dissolution of high melting point phase Mg_5(Gd,Y) in a short time and at a relatively low temperature could be rationalized by the severe deformation during FSP, which resulted in intense mixing of the α-Mg and second phase and the break-up of the eutectic (Fig. 1(b)). Consequently, the diffusion distance of the Gd and Y atoms in the Mg matrix was significantly shortened. Furthermore, the diffusion rate was believed to be remarkably accelerated during FSP [29]. These induce accelerated dissolution of the coarse second-phase particles [29].

In Fig. 1(d), a few of the spheroid and cuboid particles with a size of 0.5–3.5 μm were detected. EDS analyses revealed that they were a zirconium rich phase and a compound containing Mg, Y, and Gd, respectively (Table 1). The cuboid-shaped particles containing Mg, Gd, and Y were similar to those reported by Gao et al. [3]. They found that after the Mg_5(Gd,Y) phase was dissolved with a solution-treatment at 525 °C for 12 h, a few of the cuboid-shaped particles remained. They suggested that the cuboid-shaped phase was $Mg_2Y_3Gd_2$ based on EDS and XRD analyses. However, these particles in the present GW103 alloy could not be detected by XRD due to their low number.

Fig. 4(a) presents TEM images of the as-FSP sample. Few dislocations existed in the grain interior, which is consistent with the occurrence of DRX with the boundary migration and grain growth. Furthermore, a few of the cuboid-shaped particles were found in the α-Mg solution. The selected area electron diffraction (SAED) pattern indicated that the cuboid-shaped particles had a face-centered cubic (fcc) structure with a crystal lattice constant of 0.56 nm (as shown by insert A in Fig. 4(a)). Aside from that, only the diffraction spots of the α-Mg existed (as shown by insert B in Fig. 4(a)), confirming the fundamental dissolution of the Mg_5(Gd,Y) phase.

He et al. [15] reported similar cuboid-shaped particles with the same crystalline parameters. They deduced that the cuboid-shaped phase was Mg_5(Gd,Y) by TEM and EDS. However, the atomic ratio of Mg:Y:Gd for the present cuboid particles was 18.78:40.54:40.68 (point C, Fig. 1(d)), and obviously deviated from the results of Refs. [3,15]. Li et al. [30] suggested that $Mg_2Y_3Gd_2$ could precipitate within the Mg_5(Gd,Y) phase. Unfortunately, the lack of information about phase constitutions in Mg–Gd–Y alloys (the present powder diffraction files (PDF Cards) for XRD constitution of Mg, Gd, Y are limited) makes exact identification of the cuboid-shaped phase impossible up to this point.

A previous study [22] reported that a single-pass FSP on AZ80 castings at a FSP parameter of 400/100 produced an average grain size of 14.6 μm. It is interesting to note that although a higher heat input of 800/50 was used for the GW103 casting in this study, a smaller grain size of 6.1 μm was obtained. This is attributed to the effective pining of the Zr-rich phase and the remaining MgGY phase particles on the growth of recrystallized grains during FSP. There-

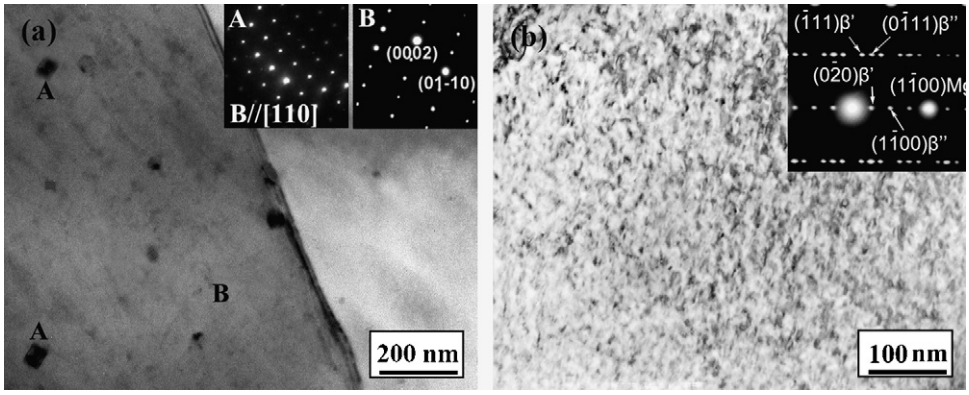

Fig. 4. TEM images of GW103 samples: (a) as-FSP and (b) FSP + aging.

fore, it is possible to produce the fine grained Mg–Gd–Y–Zr alloys by FSP at a higher heat input condition. The higher heat input condition was beneficial to the dissolution of intermetallics due to intensified stirring and higher temperatures.

For Mg–Al–Zn alloys, in order to achieve a fine grain structure, FSP under a lower heat input condition is necessary due to the absence of pinning particles. However, one pass FSP usually produced an ununiform microstructure with undissolved $Mg_{17}Al_{12}$ particle bands along the onion ring structure in the Mg–Al–Zn castings [22]. It is necessary to conduct a two-pass FSP to achieve a complete dissolution of the $Mg_{17}Al_{12}$ phase and produce a uniform microstructure. In the present GW103 alloy, a relatively homogeneous microstructure without undissolved particle bands was achieved by one pass FSP under a relatively high heat input condition, though the alternating CGBs and FGBs were observed. Therefore, it is possible to produce fine and uniform microstructure in the Mg–RE alloys by adjusting the FSP parameters.

After 13 h of post-FSP aging, the XRD patterns revealed that the peaks corresponding to the $Mg_5(Gd,Y)$ phase emerged, indicating the re-precipitation of the dissolved phase (Fig. 2(c)). It is noted that the peaks in the aged FSP sample is significantly lower than that in the as-cast sample, which is attributed to the precipitation of fine metastable phase particles. The average grain size in the SZ kept almost constant (~6.2 μm) even after aging at 225 °C (Fig. 5), compared with that of the as-FSP sample (Fig. 1(c)). TEM examinations revealed that a great number of fine particles with sizes less than ~10 nm were uniformly distributed in the α-Mg matrix (Fig. 4(b)). The SAED analyses suggested that the fine particles were the metastable β″ and β′ phases with D019 and cbco structures, respectively [31]. The crystallographic orientation relationship between β″/β′ and the Mg matrix was determined as follows: $(1\bar{1}00)_{Mg}\|(1\bar{1}00)_{\beta''}$, $[01\bar{1}0]_{Mg}\|[01\bar{1}0]_{\beta''}$ and $(\bar{1}100)_{Mg}\|(0\bar{1}0)_{\beta'}$, $[0001]_{Mg}\|[001]_{\beta'}$. It is well known that the metastable β″ and β′ phases were coherent with the matrix [6,31]. No transition β_1 phase or equilibrium β phase was detected in the grain interiors.

In Ref. [32], it was reported that the precipitation sequence at 250 °C for the Mg–Gd–Y–Zr could be described as: super-saturated solid solution (S.S.S.S.) → β″ (D019) → β′ (cbco) → β_1 (fcc) → β (fcc), while the β″ and β′ phases could coexist at peak aging status [33]. In the present study, the 13 h aging at 225 °C was close to the peak aging status [1,3,15], leading to the coexistence of the β″ and β′ phases. However, it should be noted that the β′ phase particles as reported in Refs. [15,32] were difficult to observe in the TEM image (Fig. 4(b)). It might be attributed to the limited precipitation of the β′ phase due to the lower aging temperature and shorter time in this study than those in Refs. [15,32].

DSC analyses indicated that there were three exothermic peaks in the as-FSP sample, whereas one exothermic peak and one endothermic peak were observed in the aged FSP sample (Fig. 6). The β″ and β′ phases coexisted in the peak aging condition and the β_1 phase appeared mainly at higher aging temperatures (250 and 300 °C) or in over-aging conditions [1]. It is noted that exothermic peak P1 occurred only in the as-FSP sample. Considering that the as-FSP sample is a supersaturated solid solution, exothermic peak P1 is attributed to the precipitation of the β″ or β′ phase.

In the as-FSP sample, exothermic peak P2 was observed at the temperature range of 250–300 °C, whereas endothermic peak D1 appeared at the same temperature range in the aged FSP sample. Peak P2 in the as-FSP sample corresponded to the β_1 formation in accordance with Ref. [1]. The aged FSP sample contained mainly β″

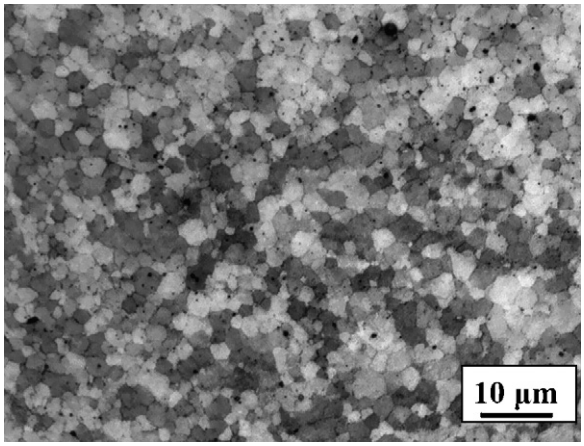

Fig. 5. Microstructure of aged FSP GW103 sample.

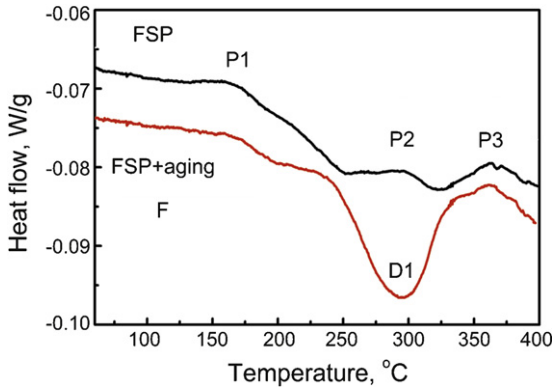

Fig. 6. DSC curves of GW103 samples in as-FSP and FSP + aging conditions.

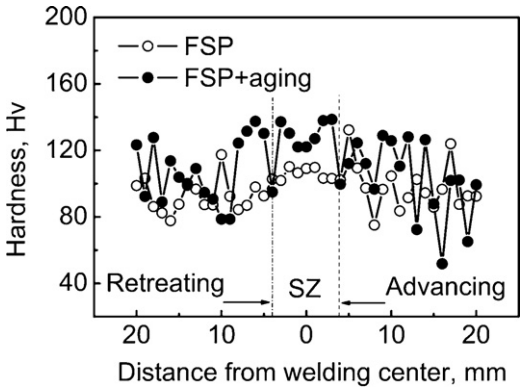

Fig. 7. Microhardness profiles of GW103 samples in as-FSP and FSP + aging conditions.

phase as well as a small amount of β′ phase as discussed above. The β′ phase was relatively stable and could exist even at an overaging stage, and the β_1 formation results from the decomposition of the β′ phase instead of the nucleation on the β″ phase [32]. Due to the limited amount of stable β′ phase, the formation of the β_1 phase was limited. Therefore, it can be concluded that endothermic peak D1 in the aged FSP sample mainly resulted from the dissolution of the β″ phase.

In both the as-FSP and aged FSP samples, exothermic peak P3 appeared, and it is associated with the formation of the equilibrium phase β. From DSC and TEM analyses, it could be concluded that the aging process in this study was close to the peak aging status, and the grains were stable during the aging process (Fig. 5). Therefore, the post-FSP aging could produce an ideal microstructure with fine grains and uniformly distributed coherent precipitates in the matrix.

Fig. 7 shows the hardness profiles on the cross-section of the FSP samples. The hardness in the BM zone of the as-FSP sample exhibited a remarkable fluctuation, with the highest hardness values being higher than those of the SZ. The hardness fluctuation of the as-cast BM was attributed to the presence of the coarse β-Mg_5(Gd,Y) phase. By comparison, the hardness of the SZ is relatively uniform and generally higher than that of the BM zone except for the high hardness points of the BM zone at the β-Mg_5(Gd,Y). This is attributed to significant grain refinement and the breakage and dissolution of most of the coarse β-Mg_5(Gd,Y) particles in the SZ zone. After post-FSP aging, both the BM and the SZ exhibit an obvious increase in the hardness resulting from the precipitation of fine β″ and β′ particles, because both the BM and the SZ are supersaturated.

Table 3 summarizes the room temperature tensile properties of the GW103 samples under various conditions. The as-cast sam-

Table 3
Tensile properties of GW103 samples under various conditions.

Sample	UTS (MPa)	YS (MPa)	El. (%)
As-cast	187	178	3.2
FSP	312	210	19
FSP + aging	439	330	3.4

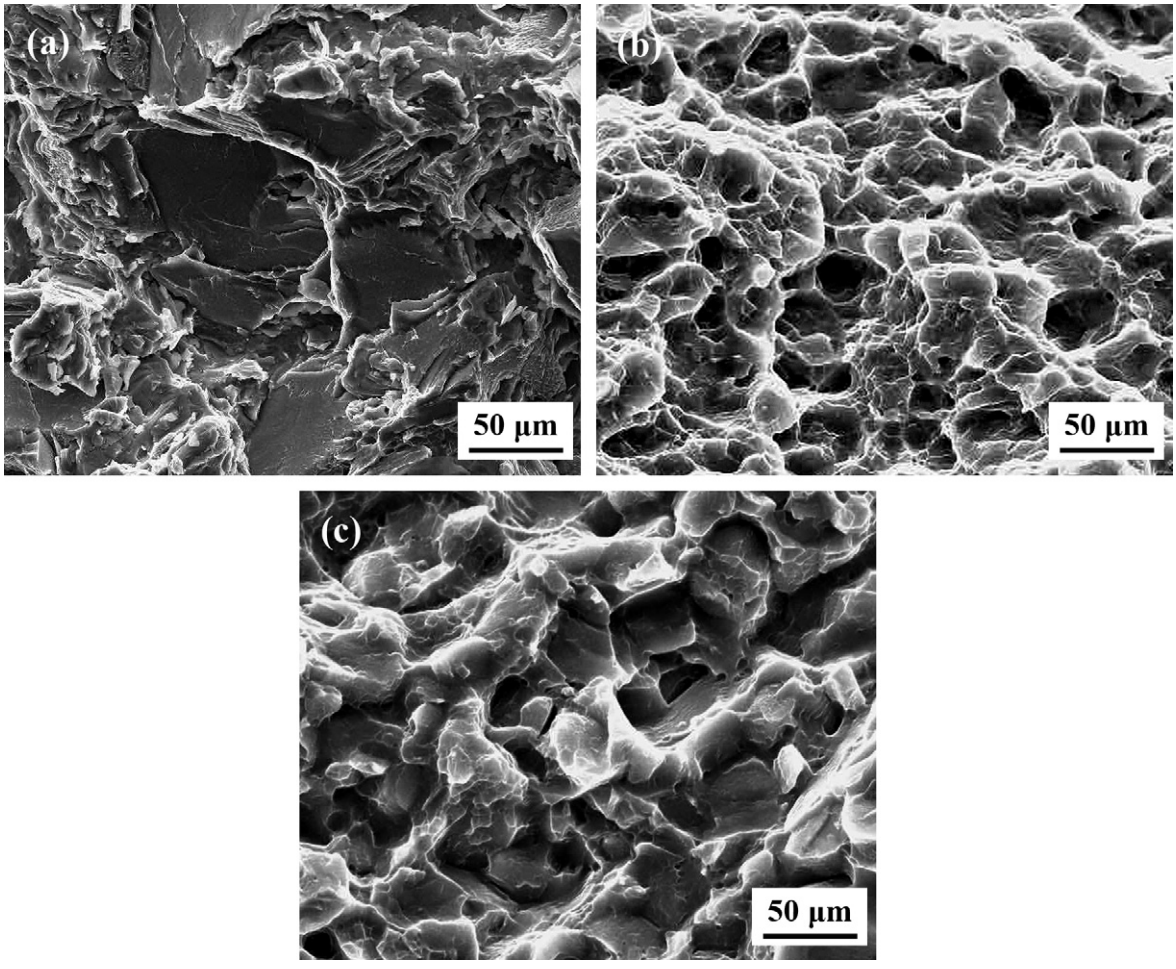

Fig. 8. SEM fractographs of GW103 samples: (a) as-cast, (b) as-FSP, (c) FSP + aging.

ple exhibited a yield strength (YS) of 178 MPa, an ultimate tensile strength (UTS) of 187 MPa, and an elongation of 3.2%. The coarse eutectic Mg_5(Gd,Y) network at the grain boundaries tended to crack or debond from the magnesium matrix early under a lower stress during tensile deformation (Fig. 8(a)). Thus, the strength and ductility are low. FSP resulted in a slightly improved YS (210 MPa) and significantly improved UTS (312 MPa) and elongation (19%). Liu et al. [1] reported that an as-extruded GW103 alloy with a pre-tempering (480 °C for 6 h) exhibited YS and UTS of 192 and 290 MPa, respectively, with an elongation of 13%. The as-extruded alloy contained streamline-like eutectics, which were broken up by extrusion with an average grain size of 9 μm. In contrast, the average grain size was finer and the number of secondary phases was fewer in the present as-FSP sample. The as-FSP sample showed better tensile properties due to the solution strengthening and microstructure refinement. The fracture surface of the as-FSP sample was characterized by equiaxed and fine dimples (Fig. 8(b)), indicating a typical dimple-fracture.

The aged FSP sample exhibited a UTS of 439 MPa, a YS of 330 MPa, and an elongation as low as 3.4%. It was reported that the precipitation strengthening of Mg alloys by prismatic precipitate plates is invariably larger than those produced by basal precipitate plates [34]. The plate-shaped β′ precipitates, formed on the prismatic planes of the matrix in a dense triangular arrangement [32], were vertical to the basal plane of the α-Mg and, together with the β″ precipitates [33], provided the most effective obstacles to the basal dislocation slip. Therefore, the strength of the aged FSP sample was significantly improved. Meanwhile, the precipitation strengthening led to the generation of stress concentration due to the dislocation being pinned up, thus micro-cracks developed along (0 0 0 1) crystal planes and cleavage fracture occurred [22], as shown in Fig. 8(c). As a result, the elongation decreased significantly due to the precipitation hardening and cleavage fracture. In a previous study by Liu et al. [1], a T5-treated (aged at 225 °C) extruded GW103 alloy exhibited a UTS of 383 MPa and a YS of 261 MPa with an elongation of 9%. In contrast, the present aged FSP sample exhibited higher strength and lower elongation. Therefore, optimizing the FSP parameters and aging procedures is necessary for improving the ductility of the FSP sample.

4. Conclusions

In summary, the following conclusions are reached:

(1) Single-pass FSP on GW103 casting caused remarkable grain refinement and fundamental dissolution of the coarse eutectic Mg_5(Gd,Y) network, thereby improving significantly the tensile properties, in particular ductility.

(2) Post-FSP aging resulted in the precipitation of the β″ and β′ phase, thereby increasing considerably the yield and tensile strengths.

(3) FSP combined with aging is an effective approach to enhancing the mechanical properties of cast Mg–Gd–Y–Zr alloy.

Acknowledgements

This work was supported by (a) the National Natural Science Foundation of China under Grant No. 50901075, (b) the National Basic Research Program of China under Grant No. 2006CB605205 and (c) the National Outstanding Young Scientist Foundation of China under Grant No. 50525103.

References

[1] X.B. Liu, R.S. Chen, E.H. Han, J. Alloys Compd. 465 (2008) 232.
[2] J.F. Nie, X. Gao, S.M. Zhu, Scripta Mater. 53 (2005) 1049.
[3] Y. Gao, Q. Wang, J. Gub, Y. Zhao, Y. Tong, Mater. Sci. Eng. A459 (2007) 117.
[4] N. Balasubramani, U.T.S. Pillai, B.C. Pai, J. Alloys Compd. 460 (2008) L6.
[5] T. Honma, T. Ohkubo, S. Kamado, K. Hono, Acta Mater. 55 (2007) 4137.
[6] T. Honma, T. Ohkubo, K. Hono, S. Kamado, Mater. Sci. Eng. A 395 (2005) 301.
[7] M.E. Drits, E.M. Padezhnova, DobakinaF T.V., Izv. Akad.Nauk. SSSR, Met. 3 (1979) 223.
[8] L. Gao, R.S. Chen, E.H. Han, J. Alloys Compd. 472 (2009) 234.
[9] K. Liu, J.H. Zhang, D.X. Tang, L.L. Rokhlin, F.M. Elkin, J. Meng. Mater. Chem. Phys. 117 (2009) 107.
[10] Y. Gao, Q.D. Wang, J.H. Gu, Y. Zhao, Y. Tong, D.D. Yin, J. Alloys Compd. 477 (2009) 374.
[11] D.J. Li, X.Q. Zeng, J. Dong, C.Q. Zhai, W.J. Ding, J. Alloys Compd. 468 (2009) 164.
[12] D.D. Yin, Q.D. Wang, Y. Gao, C.J. Chen, J. Zheng, J. Alloys Compd. (2010) 194, doi:10.1016/j.jallcom.2010.09.
[13] X.L. Hou, Q.M. Peng, Z.Y. Cao, S.W. Xu, S. Kamado, L.D. Wang, Y.M. Wu, L.M. Wang, Mater. Sci. Eng. A 520 (2009) 126.
[14] X.M. Zhang, L. Li, Y.L. Deng, N. Zhou, J. Alloys Compd. 481 (2009) 296.
[15] S.M. He, X.Q. Zeng, L.M. Peng, X. Gao, J.F. Nie, W.J. Ding, J. Alloys Compd. 427 (2007) 316.
[16] R.S. Mishra, Z.Y. Ma, Mater. Sci. Eng. R 50 (2005) 1.
[17] G.M. Xie, Z.Y. Ma, L. Geng, J. Mater. Sci. Technol. 25 (2009) 351.
[18] R.S. Mishra, M.W. Mahoney, S.X. McFadden, N.A. Mara, A.K. Mukherjee, Scripta Mater. 42 (2000) 163.
[19] C.I. Chang, C.J. Lee, J.C. Huang, Scripta Mater. 51 (2004) 509.
[20] W. Woo, H. Choo, D.W. Brown, P.K. Liaw, Z. Feng, Scripta Mater. 54 (2006) 1859.
[21] A.H. Feng, Z.Y. Ma, Scripta Mater. 56 (2007) 397.
[22] A.H. Feng, B.L. Xiao, Z.Y. Ma, Metall. Mater. Trans. A 40 (2009) 2447.
[23] A.H. Feng, Z.Y. Ma, Acta Mater. 57 (2009) 4248.
[24] T.A. Freeney, R.S. Mishra, Metall. Mater. Trans. A 41 (2010) 73.
[25] G.M. Xie, Z.Y. Ma, L. Geng, Scripta Mater. 57 (2007) 73.
[26] J.A. Schneider, A.C. Nune, Metall. Mater. Trans. B 35 (2004) 777.
[27] E. Hehmann, E. Sommer, B. Predel, Mater. Sci. Eng. A 125 (1990) 249.
[28] S. Fujie, Master's Thesis, Osaka University, Japan, 2004, p. 17.
[29] Z.Y. Ma, A.L. Pilchak, M.C. Juhas, J.C. Williams, Scripta Mater. 58 (2008) 361.
[30] L. Li, X. Zhang, Y. Deng, C. Tang, J. Alloys Compd. 485 (2009) 295.
[31] H. Karimzadeh, Ph.D. Thesis, University of Manchester, U.K., 1985.
[32] S.M. He, X.Q. Zeng, L.M. Peng, X. Gao, J.F. Nie, W.J. Ding, J. Alloys Compd. 421 (2006) 309.
[33] Z. Yang, J.P. Li, Y.C. Guo, T. Liu, F. Xia, Z.W. Zeng, M.X. Liang, Mater. Sci. Eng. A 454–455 (2007) 274.
[34] J.F. Nie, Scripta Mater. 48 (2003) 1009–1015.